



Contrast-enhanced ultrasound with dispersion analysis for the localization of prostate cancer: correlation with radical prostatectomy specimens

Arnoud W. Postema¹ · Maudy C. W. Gayet^{2,3} · Ruud J. G. van Sloun³ · Rogier R. Wildeboer³ · Christophe K. Mannaerts¹ · C. Dilara Savci-Heijink⁴ · Stefan G. Schalk³ · Amir Kajtazovic² · Henk van der Poel⁵ · Peter F. A. Mulders⁶ · Harrie P. Beerlage^{1,3} · Massimo Mischi³ · Hessel Wijkstra^{1,3}

Received: 5 September 2019 / Accepted: 21 January 2020 / Published online: 20 February 2020
© Springer-Verlag GmbH Germany, part of Springer Nature 2020

Abstract

Purpose To determine the value of two-dimensional (2D) contrast-enhanced ultrasound (CEUS) imaging and the additional value of contrast ultrasound dispersion imaging (CUDI) for the localization of clinically significant prostate cancer (csPCa).

Methods In this multicentre study, subjects scheduled for a radical prostatectomy underwent 2D CEUS imaging preoperatively. CUDI maps were generated from the CEUS recordings. Both CEUS recordings and CUDI maps were scored on the likelihood of presenting csPCa (any Gleason $\geq 4 + 3$ and Gleason $3 + 4$ larger than 0.5 mL) by five observers and compared to radical prostatectomy histopathology. An automated three-dimensional (3D) fusion protocol was used to match imaging with histopathology. Receiver operator curve (ROC) analysis was performed per observer and imaging modality.

Results 133 of 216 (62%) patients were included in the final analysis. Average area under the ROC for all five readers for CEUS, CUDI and the combination was 0.78, 0.79 and 0.78, respectively. This yields a sensitivity and specificity of 81 and 64% for CEUS, 83 and 56% for CUDI and 83 and 55% for the combination. Interobserver agreement for CEUS, CUDI and the combination showed kappa values of 0.20, 0.18 and 0.18 respectively.

Conclusion The sensitivity and specificity of 2D CEUS and CUDI for csPCa localization are moderate. Despite compressing CEUS in one image, CUDI showed a similar performance to 2D CEUS. With a sensitivity of 83% at cutoff point 3, it could become a useful imaging procedure, especially with 4D acquisition, improved quantification and combination with other US imaging techniques such as elastography.

Keywords Prostate cancer · Contrast-enhanced ultrasound · Dispersion analysis · Radical prostatectomy · Quantitative imaging

Introduction

There is a rising interest in imaging for the diagnostic pathway of men with suspected prostate cancer (PCa) [1]. The possibility of selectively detecting and localizing clinically significant PCa could prevent unnecessary benign biopsies, reduce overdiagnosis of insignificant PCa and guide localized treatments such as focal therapy (FT) [2–4].

Multiparametric magnetic resonance imaging (mpMRI) has a recognized value in the diagnostic pathway of PCa [1, 4–6]. Strategies incorporating mpMRI in patient selection and monitoring for active surveillance and guiding focal treatments are also emerging [2, 7]. However, there are also concerns relating to large-scale availability, costs and inconsistencies in reported reliability despite the prostate imaging reporting and data system (PIRADS). The negative predictive value (NPV) of mpMRI varies among studies and current guidelines do not yet recommend excluding patients from prostate biopsies on the basis of a negative mpMRI [8–14].

Ultrasound (US) imaging has certain advantages (i.e., cost-effectiveness, portability, safety and compatibility with ferromagnetic biopsy and FT equipment), and novel US

Arnoud W. Postema and Maudy Gayet contributed equally to the manuscript.

✉ Maudy C. W. Gayet
m.gayet@jzbz.nl

Extended author information available on the last page of the article

technologies have emerged that allow improved PCa visualization [15, 16]. These US modalities target different aspects of malignant tissue such as increased stiffness (US-elastography) and altered vascularity (contrast-enhanced ultrasound or CEUS) [17–20]. Prostate cancer requires angiogenesis to progress to clinically significant disease and the resultant macro- and microvascular changes are targeted by CEUS [20]. In CEUS, intravascular microbubble contrast agents are used, which allow visualization and quantification of blood flow patterns associated with malignancy [21]. Typically, the inflow and outflow of a contrast bolus are recorded one plane at a time, after which the examiner looks for increased focal enhancement [22]. These signs may be subtle and many aspects of the blood flow dynamics recorded are simply not appreciable to the naked eye. Computer-aided quantification techniques have been proposed to aid in the interpretation of CEUS, potentially improving accuracy, speeding-up reading, and decreasing user dependency [21]. Contrast ultrasound dispersion imaging (CUDI) is based on the fact that cancer-related angiogenetic vascular structures are small in diameter, compressible, highly tortuous and lack normal endothelial lining, leading to less efficient dispersion of blood/contrast [23]. Several studies in which CUDI parametric analysis was used to estimate whether pixels belonged to a pre-defined malignant or benign prostate region have shown a high classifying accuracy [24, 25]. However, the clinical value of CEUS and CUDI maps is still unclear as a diagnostic reader assessment is lacking. The aim of the present study is to determine the value of CEUS imaging and CUDI parametric maps for the localization of csPCa using radical prostatectomy (RP) specimens as reference standard. We also evaluate the interobserver variability for scoring with and without CUDI parametric maps.

Methods

This analysis included data from two ethics board approved prospective studies in two Dutch medical centres. Inclusion criteria for the studies were: men, 18 years or older with biopsy-proven PCa and scheduled for RP. Exclusion criteria were inability to provide informed consent or to safely undergo study procedures because of contraindications for the contrast agent. All men provided written informed consent. All participants underwent CEUS imaging before RP. CEUS imaging was performed in the left-lateral decubitus position using a Phillips IU22 ultrasound scanner with a C10-3V endocavity probe (Phillips Healthcare, Bothell, USA) in the Academic Medical Center (AMC) in Amsterdam and a BK type 2202 Ultrasound System with a type 8818 probe (BK Medical, Copenhagen, Denmark) in the Jeroen Bosch Hospital (JBZ) in 's Hertogenbosch. Normal B-mode scanning and volumetry was performed together

with two perpendicular B-mode sweeps required for later 3D reconstruction of the prostate (base to apex transversal view and left to right sagittal view). For CEUS recording, a contrast-specific power modulation pulse scheme at 3.5 MHz and a mechanical index of 0.06 were used on the Philips scanner and 4.0 MHz and 0.22 on the BK medical system [26]. CEUS recording started after the intravenous administration of a 2.4 mL bolus of the contrast agent SonoVue® (Bracco, Geneva) followed by a 5 mL saline flush. In each CEUS recording, the contrast inflow and outflow in one plane was recorded during 2 min. No flash replenishment was applied. To insure complete washout and proper evaluation of contrast inflow in the next plane, a minimum interval of 5 min was observed before finding the next imaging plane and administration of the next bolus. 2–4 CEUS recordings were available in each patient depending on the hospital that enrolled the patient. By default the mid-base and mid-apical plane were chosen when two planes were imaged. A basal and apical plane were included if four planes were imaged. Afterwards, CUDI maps were generated from the CEUS recordings. To generate CUDI parametric maps, first per-pixel time–intensity curves (TICs) reflecting contrast dispersion dynamics are extracted from the CEUS recordings [21]. CUDI then measures the cancer-related decrease in contrast dispersion by a spatiotemporal correlation analysis of the TICs [27]. It also provides local estimates of the Peclet number, describing the ratio between convection and dispersion [23]. Parametric maps are generated by plotting colour-coded maps highlighting areas with low dispersion (high correlation coefficient among neighbouring TICs) and high Peclet number, which indicate high tumour suspicion.

Five observers performed image interpretation: two engineers dedicated to parametric analysis of prostate CEUS, with 2 years (RW), and 3 years (RS) experience; three clinicians experienced in prostate biopsies and CEUS: AP (3 years of CEUS experience), MG (3 years of CEUS experience) and CM (1 year of CEUS experience). All observers were blinded to each other's interpretations and pathology results. Each observer was presented with the CEUS, CUDI and CEUS + CUDI images together with standard B-mode images of all patients in random order by in-house built software. The observers were asked to draw any suspicious lesions and score them on a 1–5 Likert-type scale for each imaging modality (CEUS, CUDI and B-mode).

All patients underwent RP, after which the prostate specimen was formalin fixed, sliced into 4-mm slices and cut to whole mount or 2.5 by 2.5 cm coupes. Following haematoxylin and eosin staining and immunohistochemistry when necessary, tumour outlines were then drawn on the microscopy slides by uropathologists. Prostate slices were reconstructed from the coupes and stacked to create a 3D histology model of the prostate with 3D tumour delineation using custom software [28].

Using an adaptation of the procedures described in a paper of Schalk et al., a 3D model of the prostate ultrasound was constructed using the transversal and sagittal B-mode sweeps [29]. The recorded CEUS planes were placed in this model. Subsequently, the 3D models of the histopathology and imaging were elastically registered (fused). Virtual pathology slices with tumour delineation were then generated to match the recorded CEUS planes [30]. These combinations of imaging slice and virtual pathology slice were used for the imaging performance analysis (see “Data analysis”). By using 3D registration of imaging and pathology, plane angulation mismatch and plane selection error, which usually occur when manually correlating US imaging with RP, were minimized. To take into account registration inaccuracies, we adopted a 3.6-mm error margin for matching the pathology results with imaging results in the base-to-apex axis only. The 3.6-mm error margin is based on previous experiments that showed a 1.5-mm error in pathology reconstruction and 2.1 mm in registration error [29]. For an overview of the workflow, see Fig. 1. The workflow of the study, including the in-house built software presenting the images to the observers, was tested on the pilot cohort consisting of six randomly selected patients from the cohort (see Fig. 1).

Data analysis

Axial imaging planes were divided into four quadrants by means of a consensus meeting among observers resulting in

up to 16 zones being defined per patient. For each zone, the presence of csPCa was established (Gleason $\geq 4 + 3$ lesion and Gleason 3 + 4 lesions larger than 0.5 mL). Zones with insignificant PCa were excluded from the analysis. In both imaging and pathology, tumours were allocated to a zone if at least 10% of their pixels with a minimum surface of 3 mm² lie within that zone. The imaging score for CEUS and CUDI readings was determined as follows: the 1–5 CEUS score (or CUDI score, respectively) + 0.5 in case of a B-mode suspicion of 3 or 4, and + 1 for a B-mode suspicion of 5. For the combined CEUS + CUDI reading, CEUS and CUDI scores were averaged, then 0.5 or 1 point was added for a B-mode suspicion of 3 to 4, or 5 respectively. Imaging scores over 5 were maximized to 5, resulting in a 1–5 suspicion score in 0.5 increments. For each zone, the highest imaging suspicion score allocated by the observer was compared to the pathology results. Receiver operating characteristic (ROC) curves were generated for all observers and readings (CEUS, CUDI and CEUS + CUDI) separately and pooled. Interobserver variability was calculated by means of a weighted Fleiss Kappa statistic.

Results

216 patients (99 from the AMC and 117 from the JBZ) underwent preoperative CEUS scanning between 2013 and 2016. As presented in the flowchart, 133 patients could be included for final analysis (Fig. 2). Of the 78 patients finally

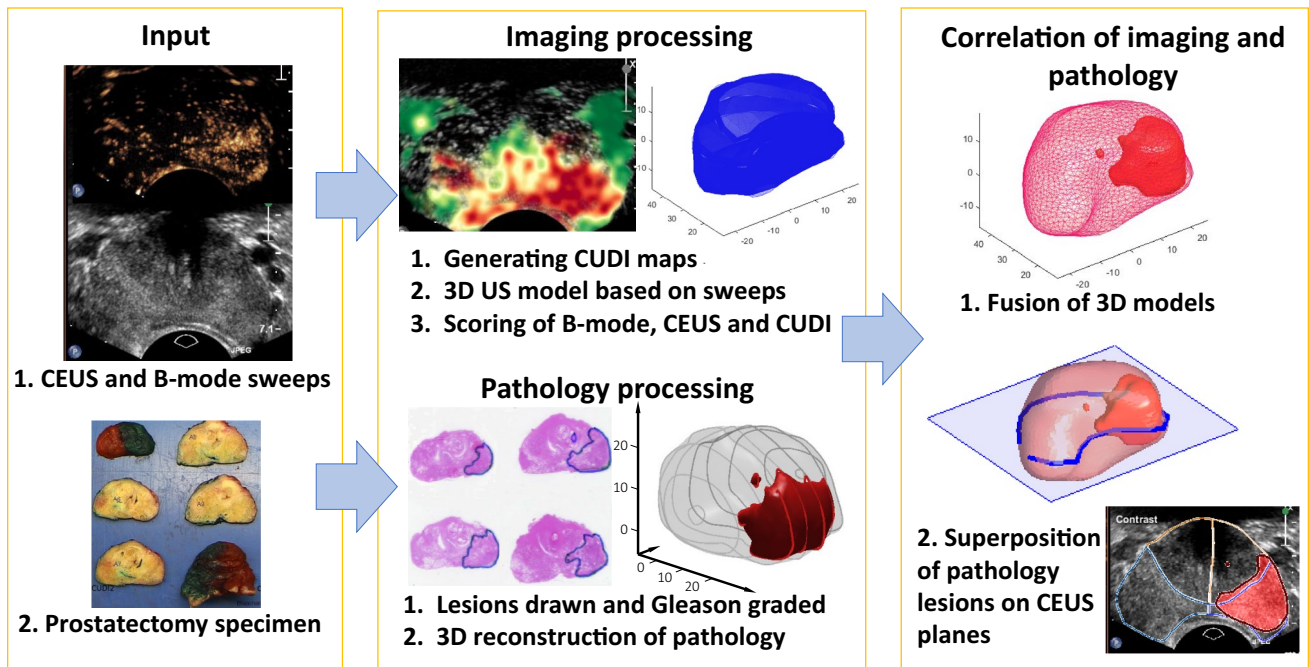


Fig. 1 Study procedures. CEUS contrast-enhanced ultrasound, CUDI contrast ultrasound dispersion imaging, US ultrasound

Fig. 2 Flowchart. *AMC* Academic Medical Center, *JBZ* Jeroen Bosch Ziekenhuis, *SNR* signal to noise ratio

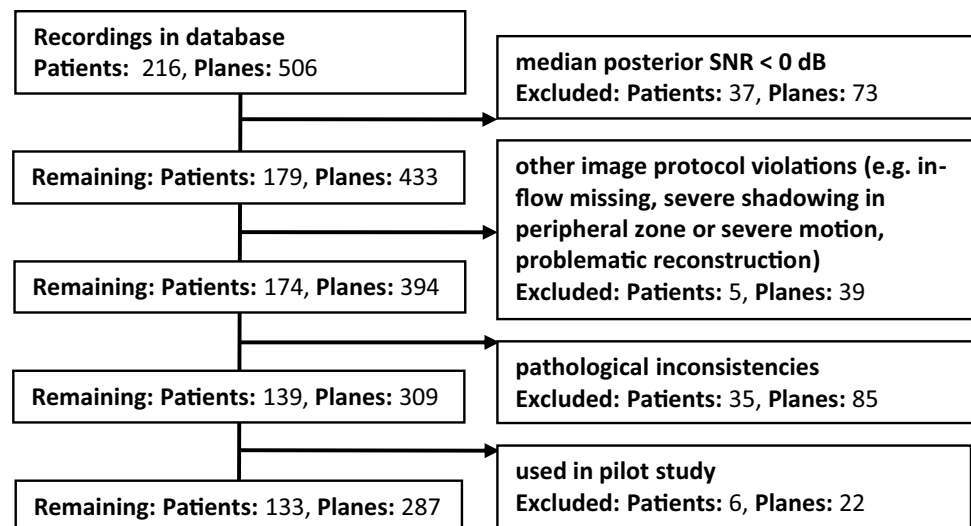


Table 1 Patient characteristics

	AMC+JBZ
Total patients (<i>n</i>)	133
Mean age in years, (range) [years]	63 (64; 37–83)
Median PSA in ng/mL, (range) [ng/mL]	5.8 (2.6–67)
Median prostate volume in ml, (range)	37 (10–118)
Clinical T-stage, <i>n</i> (%)	
T1	52 (39%)
T2	60 (45%)
T3	21 (16%)
Biopsy grade group, <i>n</i> (%)	
1	67 (50%)
2	41 (31%)
3	10 (8%)
4	8 (6%)
5	7 (5%)
Pathological T stage, <i>n</i> (%)	
pT2a	18 (14%)
pT2b	7 (5%)
pT2c	73 (55%)
pT3a	25 (19%)
PT3b	10 (8%)
Prostatectomy grade group, <i>n</i> (%)	
1	44 (33%)
2	51 (38%)
3	20 (15%)
4	9 (7%)
5	9 (7%)

included in the AMC, 42 underwent their RP at the Antoni van Leeuwenhoek Hospital (Amsterdam, The Netherlands). The baseline descriptive statistics of the population are presented in Table 1. AUC values are presented in Table 2.

Table 2 AUC values per observer

	CEUS	CUDI	CEUS+CUDI
Observer 1	0.82	0.79	0.82
Observer 2	0.79	0.81	0.80
Observer 3	0.74	0.75	0.74
Observer 4	0.79	0.80	0.77
Observer 5	0.79	0.78	0.78
Average	0.78	0.79	0.78

CEUS contrast-enhanced ultrasound, *CUDI* contrast ultrasound dispersion imaging

Average AUC for all five readers for CEUS, CUDI and the combination are 0.78, 0.79 and 0.78, respectively. An ROC curve for the pooled scores is presented in Fig. 3. Pooled sensitivity and specificity for all five readers, per cutoff value and imaging modality, are presented in Table 3. Average performance for CEUS, CUDI and the combination of CEUS and CUDI was comparable. Kappa scores for interobserver agreement for CEUS, CUDI and CEUS+CUDI are 0.20, 0.18 and 0.18, respectively, indicating poor interobserver agreement.

Discussion

In our study, employing quantitative analysis using CUDI maps resulted in similar tumour localization performance as qualitative analysis using 2D CEUS recordings. Providing the observers with both CEUS recordings and CUDI maps did not lead to a better performance. However, the observers had gained considerable prior experience with CEUS interpretation during image acquisition for the current study and other CEUS projects, while CUDI images were

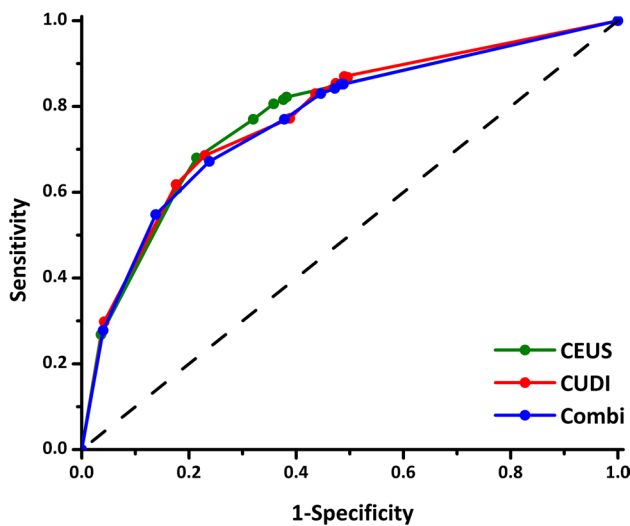


Fig. 3 Receiver operator characteristic curve for all CEUS, CUDI and the combination using pooled data from all five observers. Area under the curve is 0.78 for CEUS, 0.79 for CUDI and 0.78 for the combination. *CEUS* contrast-enhanced ultrasound, *CUDI* contrast ultrasound dispersion imaging

relatively new to them. This might explain why (the addition of) CUDI did not result in a better classifying performance above CEUS reading only. Specificity was decreased by providing both CEUS and CUDI, which may be explained by a higher number of false positives resulting from more potentially suspicious visual cues being presented. Interobserver agreement was poor in general. Contrary to our expectations, CUDI did not improve interobserver agreement compared to CEUS imaging. The disparity between the reasonably good AUCs achieved by the individual reader, but poor interobserver agreement points towards different accurate assessments and mistakes being made by the readers. A structured training programme might overcome this limitation in the future. Besides equal performance in localizing PCa to 2D CEUS, there are several possible advantages of CUDI compressing all the information of a CEUS video in a single image such as possibly shorter reading time (not measured in current study), low data consumption on storage devices/networks and easy file transfer.

Our results compare favourably with the very limited published data that compare CEUS imaging results with RP pathology. Three limited studies comprising 12, 13 and 50

patients report sensitivities of 38–42%, but no specificities [31–33]. A 2011 study by Seitz et al. report a per-patient sensitivity, specificity PPV and NPV of 71%, 50%, 92% and 18%, respectively [22]. Since we performed a per-ROI analysis instead of a per-patient analysis, these results cannot be directly compared. Biopsy-based studies have shown improved detection rates by adding CEUS-targeted cores to systematic biopsy regimens, but insufficient accuracy to obviate systematic cores altogether [4].

Because mpMRI is now the mainstay of PCa imaging, emerging imaging technologies like CEUS should be compared with mpMRI. Unfortunately, in the current cohort, no standard mpMRI was performed preoperatively. No direct comparison between CEUS and mpMRI using RP specimens has been published to date. However, a biopsy study comparing CEUS-targeted and MRI-targeted biopsy will be published shortly [34]. The reported performance of mpMRI varies widely depending on the study design, population, method of correlating imaging with pathology and definitions in image interpretation. A meta-analysis including studies using RP specimens of template biopsies as reference standard reports sensitivities of 80–90% with specificities of 50–90% [35]. However, some studies with a (considerably) lower performance have been published [36, 37].

Our study was limited by the fact that we did not perform whole prostate imaging. For logistical reasons, a varying number of planes were recorded per patient. The number of planes scanned was not influenced by PCa risk factors or tumour visualization, but purely dependent on protocolized trial logistics. Scanning the entire prostate was unfeasible because with 2D CEUS inflow and outflow of contrast bolus have to be recorded per plane, each plane requiring a new bolus and 5 min for contrast inflow and washout. Another limitation lies in the statistical analysis that does not take clustering of the data on the per-patient and reader level into account. Moreover, 38% of patients had to be excluded from the final analysis, mainly because of pathology protocol violations and, in the JBZ, because of insufficient ultrasound quality (especially shadowing).

The 3D fusion method we used had to cope with inconsistent manual slicing of the prostate specimen and the suboptimal method of 3D reconstruction of the prostate images using manual 2D sweeps. The 3.6-mm error margin we used in assigning the histopathology to each quadrant was more conservative than similar strategies other

Table 3 Pooled sensitivity and specificity for five observers rating likelihood of significant PCa presence on a 1–5 Likert scale on CEUS imaging, CUDI and the combination of both

	Cutoff value 3			Cutoff value 3.5			Cutoff value 4		
	CEUS	CUDI	Combi	CEUS	CUDI	Combi	CEUS	CUDI	Combi
Sens	0.81	0.83	0.83	0.77	0.77	0.77	0.68	0.69	0.68
Spec	0.64	0.56	0.55	0.68	0.63	0.62	0.79	0.77	0.77

CEUS = contrast-enhanced ultrasound, CUDI = contrast ultrasound dispersion imaging

authors have used to compensate for imaging to pathology mismatch. However, one cannot be certain whether over- or under-compensation has occurred [36, 38]. Without this compensation, average AUC would be 0.66, 0.65 and 0.65 for CEUS, CUDI and the combination, respectively. There are two additional limitations to our study that are likely to have suppressed the classification performance. (1) The observers received no systematic training with feedback to read CEUS or CUDI. This may also have contributed to the high interobserver variability. (2) The algorithm we used to combine CEUS, CUDI and B-mode scores into a single imaging score was arbitrarily chosen before data analysis. Further research will have to establish and validate the optimal method of combining scores for different ultrasound imaging modalities. As with most studies using radical prostatectomy specimens as the reference standard, generalizability of results towards the pre-diagnosis population is limited due to spectrum bias (all our included patients have PCa). We propose future work on (ultrasound) PCa imaging to use an optimized method of correlating imaging with pathology. For example, the use of 3D moulds or devices that ensure precise and consistent prostate slicing will improve the accuracy of the gold standard for future studies [38]. Also, the acquisition of imaging in 3D will likely improve ultrasound to pathology matching as the 3D reconstruction of 2D images inevitably leads to error. Scanners that allow 4D (3D + time) CEUS acquisition are now available. Since blood flow anomalies targeted by CEUS are a 4D phenomenon, it is conceivable that recording and analysing these in 4D will also improve quantification and diagnostic accuracy [39]. Furthermore, 4D CEUS will enable scanning the entire gland using a single bolus of contrast making it easy to incorporate whole gland imaging in clinical workflows.

With an average classification performance of approximately 0.78 (average AUC), our current 2D CEUS and CUDI imaging procedures seem to have insufficient diagnostic power to be used as a stand-alone tool for PCa imaging. Besides the important previously mentioned step towards 4D, ongoing research to improve CUDI is dedicated to developing new parameters that can be extracted from CEUS and combining existing ones [24, 37]. Like in mpMRI, the discrimination between benign and malignant prostate tissue could be improved by assessing multiple tissue features besides (micro)vascularization. Combining CEUS/CUDI with complementary features, such as tissue stiffness measured by ultrasound elastography, can be considered to improve the diagnostic accuracy through a multiparametric ultrasound (mpUS) approach [40]. One study group has used CEUS to further characterize lesions found with elastography cutting their false positives from 35 to 10%, while only 7% of confirmed tumours showed normal CEUS perfusion patterns [41]. Results of a more comprehensive

study correlating CEUS and shear wave elastography with RP specimens are expected shortly [42].

Conclusion

The sensitivity and specificity of 2D CEUS and CUDI for csPCa localization are moderate with an average AUC of 0.78. Despite compressing CEUS in one image, CUDI showed a similar performance to 2D CEUS. With a sensitivity of 83% at cutoff point 3, it could become a useful imaging procedure. Future research should focus on 4D acquisition, improved quantification and combination with other US imaging techniques such as elastography, and direct comparison with mpMRI.

Acknowledgements This research project was supported by a grant from the Dutch Cancer Society (KWF Kankerbestrijding grant UVA 2013-5941). This study was performed within the framework of CTMM, The Center for Translational Molecular Medicine, PCMM project (Grant 03O-203).

Author contributions AWP: data collection and management, data analysis, manuscript writing/editing. MG: data collection and management, data analysis, manuscript writing/editing. RJGS: data collection, data analysis. RRW: data collection, data analysis. CKM: data collection. CDS-H: data collection. SGS: data collection. AK: manuscript writing and editing. HP: data collection. PFAM: project development. HPB: project development, manuscript editing. MM: project development, manuscript editing. HW: project development, manuscript editing.

Funding This study was funded by a grant from the Dutch Cancer Society (KWF Kankerbestrijding grant UVA 2013-5941). This study was performed within the framework of CTMM, the Center for Translational Molecular Medicine, PCMM project (Grant 03O-203).

Compliance with ethical standards

Conflict of interest The authors declare that they have no conflict of interest.

Ethical approval All procedures performed in studies involving human participants were in accordance with the ethical standards of the institutional and/or national research committee (Medisch Ethische Toetsingscommissie AMC and Medisch Ethische Toetsingscommissie Brabant) and with the 1964 Helsinki Declaration and its later amendments or comparable ethical standards.

Informed consent Informed consent was obtained from all individual participants included in the study.

References


1. Mottet N, Bellmunt J, Bolla M, Briers E, Cumberbatch MG, Santis M et al (2017) EAU-ESTRO-SIOG guidelines on prostate cancer. Part 1: screening, diagnosis, and local treatment with curative intent. *Eur Urol* 71(4):618–629

2. Schulman AA, Sze C, Tsivian E, Gupta RT, Moul JW, Polascik TJ (2017) The contemporary role of multiparametric magnetic resonance imaging in active surveillance for prostate cancer. *Curr Urol Rep* 18(7):52
3. van den Bos W, Muller BG, Ehdaie B, Scardino P, de la Rosette JJ (2014) What is still needed to make focal therapy an accepted segment of standard therapy? *Curr Opin Urol* 24(3):247–255
4. van Hove A, Savoie PH, Maurin C, Brunelle S, Gravis G, Salem N et al (2014) Comparison of image-guided targeted biopsies versus systematic randomized biopsies in the detection of prostate cancer: a systematic literature review of well-designed studies. *World J Urol* 32(4):847–858
5. Haider MA, Yao X, Loblaw A, Finelli A (2016) Multiparametric magnetic resonance imaging in the diagnosis of prostate cancer: a systematic review. *Clin Oncol (R Coll Radiol)* 28(9):550–567
6. Schoots IG, Roobol MJ, Nieboer D, Bangma CH, Steyerberg EW, Hunink MG (2015) Magnetic resonance imaging-targeted biopsy may enhance the diagnostic accuracy of significant prostate cancer detection compared to standard transrectal ultrasound-guided biopsy: a systematic review and meta-analysis. *Eur Urol* 68(3):438–450
7. Bjurlin MA, Mendhiratta N, Wysock JS, Taneja SS (2016) Multiparametric MRI and targeted prostate biopsy: improvements in cancer detection, localization, and risk assessment. *Cent Eur J Urol* 69(1):9–18
8. Billing A, Buchner A, Stief C, Roosen A (2016) Poor standard mp-MRI and routine biopsy fail to precisely predict intraprostatic tumor localization. *World J Urol* 34(10):1383–1388
9. Filson CP, Natarajan S, Margolis DJ, Huang J, Lieu P, Dorey FJ et al (2016) Prostate cancer detection with magnetic resonance-ultrasound fusion biopsy: the role of systematic and targeted biopsies. *Cancer* 122(6):884–892
10. Hutchinson R, Lotan Y (2017) Cost consideration in utilization of multiparametric magnetic resonance imaging in prostate cancer. *Transl Androl Urol* 6(3):345–354
11. Moldovan PC, Van den Broeck T, Sylvester R, Marconi L, Bellmunt J, van den Bergh RCN et al (2017) What is the negative predictive value of multiparametric magnetic resonance imaging in excluding prostate cancer at biopsy? A systematic review and meta-analysis from the European Association of Urology Prostate Cancer Guidelines Panel. *Eur Urol* 72(2):250–266
12. Schouten MG, van der Leest M, Pokorny M, Hoogenboom M, Barentsz JO, Thompson LC et al (2017) Why and where do we miss significant prostate cancer with multi-parametric magnetic resonance imaging followed by magnetic resonance-guided and transrectal ultrasound-guided biopsy in biopsy-naive men? *Eur Urol* 71(6):896–903
13. Sonn GA, Fan RE, Ghanouni P, Wang NN, Brooks JD, Loening AM et al (2017) Prostate magnetic resonance imaging interpretation varies substantially across radiologists. *Eur Urol Focus* 5:592–599
14. Schoots IG (2016) Omission of systematic transrectal ultrasound guided biopsy from the MRI targeted approach in men with previous negative prostate biopsy might still be premature. *Ann Transl Med* 4(10):205
15. Mitterberger M, Horninger W, Aigner F, Pinggera GM, Steppan I, Rehder P et al (2010) Ultrasound of the prostate. *Cancer Imaging* 10:40–48
16. Pavlovich CP, Cornish TC, Mullins JK, Fradin J, Mettee LZ, Connor JT et al (2014) High-resolution transrectal ultrasound: pilot study of a novel technique for imaging clinically localized prostate cancer. *Urol Oncol* 32(1):34 e27–34 e32
17. Correas JM, Tissier AM, Khairoune A, Khoury G, Eiss D, Helenon O (2013) Ultrasound elastography of the prostate: state of the art. *Diagn Interv Imaging* 94(5):551–560
18. Correas JM, Tissier AM, Khairoune A, Vassiliu V, Mejean A, Helenon O et al (2015) Prostate cancer: diagnostic performance of real-time shear-wave elastography. *Radiology* 275(1):280–289
19. Good DW, Stewart GD, Hammer S, Scanlan P, Shu W, Phipps S et al (2014) Elasticity as a biomarker for prostate cancer: a systematic review. *BJU Int* 113(4):523–534
20. Russo G, Mischi M, Scheepens W, Rosette JJ, Wijkstra H (2012) Angiogenesis in prostate cancer: onset, progression and imaging. *BJU Int* 110(11 Pt C):E794–E808
21. Postema A, Idzenga T, Mischi M, Frinking P, de la Rosette J, Wijkstra H (2015) Ultrasound modalities and quantification: developments of multiparametric ultrasonography, a new modality to detect, localize and target prostatic tumors. *Curr Opin Urol* 25(3):191–197
22. Seitz M, Gratzke C, Schlenker B, Buchner A, Karl A, Roosen A et al (2011) Contrast-enhanced transrectal ultrasound (CE-TRUS) with cadence-contrast pulse sequence (CPS) technology for the identification of prostate cancer. *Urol Oncol* 29(3):295–301
23. Mischi M, Kuenen MP, Wijkstra H (2012) Angiogenesis imaging by spatiotemporal analysis of ultrasound contrast agent dispersion kinetics. *IEEE Trans Ultrason Ferroelectr Freq Control* 59(4):621–629
24. van Sloun RJ, Demi L, Postema AW, de la Rosette JJ, Wijkstra H, Mischi M (2017) Ultrasound-contrast-agent dispersion and velocity imaging for prostate cancer localization. *Med Image Anal* 35:610–619
25. Wildeboer RR, Postema AW, Demi L, Kuenen MPJ, Wijkstra H, Mischi M (2017) Multiparametric dynamic contrast-enhanced ultrasound imaging of prostate cancer. *Eur Radiol* 27(8):3226–3234
26. Wink M, Frauscher F, Cosgrove D, Chapelon JY, Palwein L, Mitterberger M et al (2008) Contrast-enhanced ultrasound and prostate cancer; a multicentre European research coordination project. *Eur Urol* 54(5):982–992
27. Kuenen MP, Saidov TA, Wijkstra H, de la Rosette JJ, Mischi M (2013) Spatiotemporal correlation of ultrasound contrast agent dilution curves for angiogenesis localization by dispersion imaging. *IEEE Trans Ultrason Ferroelectr Freq Control* 60(12):2665–2669
28. Wildeboer RR (2017) Three-dimensional histopathological reconstruction as a reliable ground truth for prostate cancer studies. *Biomed Phys Eng Express* 3:035014
29. Schalk SG, Postema A, Saidov TA, Demi L, Smeenge M, de la Rosette JJ et al (2016) 3D surface-based registration of ultrasound and histology in prostate cancer imaging. *Comput Med Imaging Graph* 47:29–39
30. Wildeboer RR, van Sloun RJG, Postema AW, Mannaerts CK, Gayet M, Beerlage HP et al (2018) Accurate validation of ultrasound imaging of prostate cancer: a review of challenges in registration of imaging and histopathology. *J Ultrasound* 21(3):197–207
31. Halpern EJ, McCue PA, Aksnes AK, Hagen EK, Frauscher F, Gomella LG (2002) Contrast-enhanced US of the prostate with Sonazoid: comparison with whole-mount prostatectomy specimens in 12 patients. *Radiology* 222(2):361–366
32. Matsumoto K, Nakagawa K, Hashiguchi A, Kono H, Kikuchi E, Nagata H et al (2010) Contrast-enhanced ultrasonography of the prostate with Sonazoid. *Jpn J Clin Oncol* 40(11):1099–1104
33. Sano F, Terao H, Kawahara T, Miyoshi Y, Sasaki T, Noguchi K et al (2011) Contrast-enhanced ultrasonography of the prostate: various imaging findings that indicate prostate cancer. *BJU Int* 107(9):1404–1410
34. Postema AW, Scheltema MJ, Mannaerts CK, Van Sloun RJ, Idzenga T, Mischi M et al (2017) The prostate cancer detection rates of CEUS-targeted versus MRI-targeted versus systematic

- TRUS-guided biopsies in biopsy-naive men: a prospective, comparative clinical trial using the same patients. *BMC Urol* 17(1):27
35. Toner L, Weerakoon M, Bolton DM, Ryan A, Katelaris N, Lawrentschuk N (2015) Magnetic resonance imaging for prostate cancer: comparative studies including radical prostatectomy specimens and template transperineal biopsy. *Prostate Int* 3(4):107–114
 36. Isebaert S, Van den Bergh L, Haustermans K, Joniau S, Lerut E, De Wever L et al (2013) Multiparametric MRI for prostate cancer localization in correlation to whole-mount histopathology. *J Magn Reson Imaging* 37(6):1392–1401
 37. Toner L, Papa N, Perera M, Katelaris N, Weerakoon M, Chin K et al (2017) Multiparametric magnetic resonance imaging for prostate cancer—a comparative study including radical prostatectomy specimens. *World J Urol* 35(6):935–941
 38. Turkbey B, Mani H, Shah V, Rastinehad AR, Bernardo M, Pohida T et al (2011) Multiparametric 3T prostate magnetic resonance imaging to detect cancer: histopathological correlation using prostatectomy specimens processed in customized magnetic resonance imaging based molds. *J Urol* 186(5):1818–1824
 39. Wildeboer RR, Van Sloun RJG, Schalk SG, Mannaerts CK, Van Der Linden JC, Huang P et al (2018) Convective-dispersion modeling in 3D contrast-ultrasound imaging for the localization of prostate cancer. *IEEE Trans Med Imaging* 37(12):2593–2602
 40. Grey A, Ahmed HU (2016) Multiparametric ultrasound in the diagnosis of prostate cancer. *Curr Opin Urol* 26(1):114–119
 41. Brock M, Eggert T, Palisaar RJ, Roghmann F, Braun K, Loppenberg B et al (2013) Multiparametric ultrasound of the prostate: adding contrast enhanced ultrasound to real-time elastography to detect histopathologically confirmed cancer. *J Urol* 189(1):93–98
 42. Mannaerts CK, Wildeboer RR, Postema AW, Hagemann J, Budaus L, Tilki D et al (2018) Multiparametric ultrasound: evaluation of greyscale, shear wave elastography and contrast-enhanced ultrasound for prostate cancer detection and localization in correlation to radical prostatectomy specimens. *BMC Urol* 18(1):98

Publisher's Note Springer Nature remains neutral with regard to jurisdictional claims in published maps and institutional affiliations.

Affiliations

Arnoud W. Postema¹ · Maudy C. W. Gayet^{2,3}  · Ruud J. G. van Sloun³ · Rogier R. Wildeboer³ · Christophe K. Mannaerts¹ · C. Dilara Savci-Heijink⁴ · Stefan G. Schalk³ · Amir Kajtazovic² · Henk van der Poel⁵ · Peter F. A. Mulders⁶ · Harrie P. Beerlage^{1,3} · Massimo Mischi³ · Hessel Wijkstra^{1,3}

Arnoud W. Postema
a.w.postema@amc.uva.nl

Ruud J. G. van Sloun
R.J.G.v.Sloun@tue.nl

Rogier R. Wildeboer
R.R.Wildeboer@tue.nl

Christophe K. Mannaerts
c.k.mannaerts@amc.uva.nl

C. Dilara Savci-Heijink
c.d.savciheijink@amc.uva.nl

Stefan G. Schalk
S.G.Schalk@tue.nl

Amir Kajtazovic
a.kajtazovic@jzbz.nl

Henk van der Poel
h.vd.poel@nki.nl

Peter F. A. Mulders
p.mulders@uro.umcn.nl

Harrie P. Beerlage
h.p.beerlage@amc.uva.nl

Massimo Mischi
M.Mischi@tue.nl

Hessel Wijkstra
H.Wijkstra@tue.nl

¹ Department of Urology, Amsterdam University Medical Center, University of Amsterdam, Amsterdam, The Netherlands

² Department of Urology, Jeroen Bosch Hospital, Jeroen Bosch Ziekenhuis, Henri Dunantstraat 1, 5223 GZ 's Hertogenbosch, The Netherlands

³ Department of Electrical Engineering, Eindhoven University of Technology, Eindhoven, The Netherlands

⁴ Department of Pathology, Amsterdam University Medical Center, University of Amsterdam, Amsterdam, The Netherlands

⁵ Department of Urology, Netherlands Cancer Institute, Amsterdam, The Netherlands

⁶ Department of Urology, Radboud University Medical Center, Nijmegen, The Netherlands